

Mutual Capture of Dipolar Molecules at Low and Very Low Energies. II. Numerical Study

M. Auzinsh,[†] E. I. Dashevskaya,^{‡,§} I. Litvin,^{‡,§} E. E. Nikitin,^{‡,§} and J. Troe^{*,§,||}

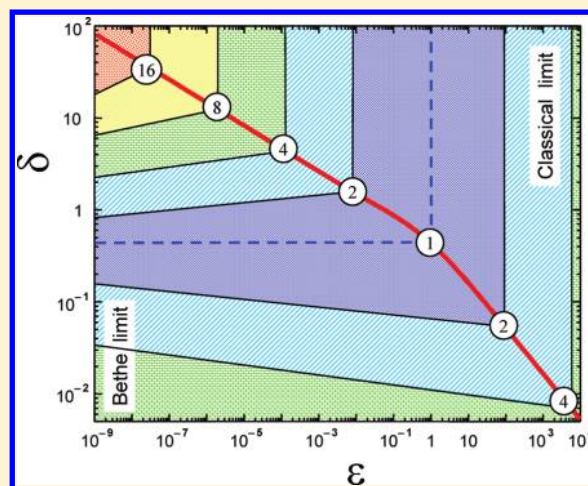
[†]Department of Physics, University of Latvia, Riga LV-1586, Latvia,

[‡]Schulich Faculty of Chemistry, Technion—Israel Institute of Technology, Haifa 32000, Israel

[§]Max-Planck-Institut für Biophysikalische Chemie, Am Fassberg 11, Göttingen D-37077, Germany

^{||}Institut für Physikalische Chemie, Universität Göttingen, Tammannstrasse 6, Göttingen D-37077, Germany

ABSTRACT: The low-energy rate coefficients of capture of two identical dipolar polarizable rigid rotors in their lowest nonresonant ($j_1 = 0$ and $j_2 = 0$) and resonant ($j_1 = 0, 1$ and $j_2 = 1, 0$) states are calculated accurately within the close-coupling (CC) approach. The convergence of the quantum rate coefficients to their quantum-classical counterparts is studied. A comparison of the present accurate numerical with approximate analytical results (Nikitin, E. E.; Troe, J. *J. Phys. Chem. A* **2010**, *114*, 9762) indicates a good performance of the previous approach which was based on the interpolation between s-wave fly wheel quantal and all-wave classical adiabatic channel limits. The results obtained apply as well to the formation of transient molecular species in the encounter of two atoms at very low collision energy interacting via resonance dipole–dipole interaction.



1. INTRODUCTION

In part I of this work¹ we have presented an analytical approximation to the low-energy rate coefficient for mutual capture of two identical dipolar diatoms in their rotational ground (non-resonant, $j_1 = j_2 = 0$) and first excited (resonant, $j_1 = 0, 1, j_2 = 1, 0$) states. The analytical treatment relied on the limiting cases of a perturbed-rotor (PR) approach: the adiabatic channel (AC) approximation for the capture of dipoles in the classical limit and the fly wheel (FW) approximation in the quantum limit of s-wave capture. The limits were based on the jmJ and the $j|J$ representations, respectively, and they were used for an interpolation such that one gets approximate expressions for capture rate coefficients from zero energy to energies in the classical domain. In the present work we use a close-coupling (CC) treatment for the capture that describes the quantum fall of the system onto an attractive center, accompanied by the locking of the intrinsic angular momentum to the collision axis. In this respect, the present paper extends our previous work on radial^{2,3} and rotational^{4,5} nonadiabatic effects within classical locking dynamics. Compared to the latter case, here we now go beyond the coupled states (CS) model which assumes the conservation of the R -helicity in a given channel.^{6,7} We also study the convergence of the accurate rate coefficients to their high-energy counterparts and assess the accuracy of the analytical approximation proposed in ref 1.

The plan of this paper is the following. In section 2 we characterize the long-range interaction between two polarizable dipoles in the perturbed rotor approximation. Section 3 presents the calculation of quantum rate coefficients for partners in rotational states $j_1 = 0$ and $j_2 = 0$ (00 manifold of channels). In section 4, the coupled-channel approach for capture of partners in rotational states $j_1 = 0$ and $j_2 = 1$ (01 manifold of channels) is described. Section 5 presents zero-energy and high-energy limiting rate coefficients, and section 6 provides the bridge between these limits and, for representative cases, shows a comparison of numerical and analytical results. Section 7 gives a general discussion as exemplified by two case studies, and section 8 concludes the paper.

2. LONG-RANGE INTERACTION BETWEEN TWO POLARIZABLE DIPOLES AND THE CORRESPONDING AC POTENTIALS

The long-range part of the interaction between two polarizable dipoles consists of a dispersion contribution V^{disp} and a dipole–dipole component $V^{\text{dip-dip}}$ (we neglect here the induction energy which typically is small⁹). Normally, the isotropic part of the dispersion interaction is much larger than the

Received: December 21, 2010

Published: May 02, 2011

anisotropic part such that the latter will be neglected and V^{disp} is written as

$$V^{\text{disp}}(R) = -C_6/R^6 \quad (2.1)$$

where R is the distance between the centers of mass of the dipoles. In turn, $V^{\text{dip.}-\text{dip.}}$ is totally anisotropic and reads

$$V^{\text{dip}-\text{dip}}(\mathbf{R}, \mathbf{d}_1, \mathbf{d}_2) = \frac{\mathbf{d}_1 \cdot \mathbf{d}_2 - 3(\mathbf{d}_1 \cdot \hat{\mathbf{r}})(\mathbf{d}_2 \cdot \hat{\mathbf{r}})}{R^3} \quad (2.2)$$

where \mathbf{d}_1 and \mathbf{d}_2 are the dipole moment vectors of rotors 1 and 2 and $\hat{\mathbf{r}}$ is the unit vector directed along the collision axis \mathbf{R} . In our work we express the interaction in eqs 2.1 and 2.2 in first and second order in the basis functions $|jm\rangle$ that correspond to the AC approach within the PR approximation. The latter considers the quantum number of the intrinsic angular momentum j as a good quantum number. Since in the following we only consider channels belonging to the 00 and 01 manifolds, j can be regarded as the quantum number of a single rotor, being either $j = 0$ or $j = 1$. The additional quantum numbers for the AC potentials are the projection of j onto \mathbf{R} , $m = 0, \pm 1$, and the quantum number $p = \pm 1$ that specifies the symmetry with respect to the permutation of two rotors.

The AC interaction potentials for nonresonant (00) and resonant (01 and 10) channels read as¹

$$V^{00}(R) = -\frac{C_6}{R^6} - \frac{d^4}{6BR^6} \quad (2.3)$$

$$V_m^{01,p}(R) = -\frac{C_6}{R^6} - \frac{2d^4}{27BR^6} + (3m^2 - 2) \left[p \frac{d^2}{3R^3} + \frac{d^4}{270BR^6} \right] \quad (2.4)$$

where B is the rotational constant of the rotors (in energy units). The terms proportional to d^4 in eqs 2.3 and 2.4 are the second-order dipole–dipole corrections with respect to free rotor states that correspond to the coupling $j = 0 \rightarrow j' = 1$ and $j = 1 \rightarrow j' = 0, 2$, respectively. The term proportional to d^2 is the first-order dipole–dipole interaction. For simplicity, we neglect the small correction proportional to d^4 in the square brackets in eq 2.4 and we rewrite the preceding equations as

$$V^{00}(R) = -\frac{C_6^{00}}{R^6} \quad (2.5)$$

$$V_m^{01,p}(R) = -\frac{C_6^{01}}{R^6} + (3m^2 - 2)p \frac{d^2}{R^3} \quad (2.6)$$

3. CAPTURE IN THE NONRESONANT MANIFOLD (00)

Following ref 10, in this section we introduce a reduced distance $\rho = R/R_6^{00}$ with $R_6^{00} = (2\mu C_6^{00}/\hbar^2)^{1/4}$ and a reduced energy $v = V/E_6^{00}$ with $E_6^{00} = \hbar^2/\mu(R_6^{00})^2$ such that the reduced wave vector κ is expressed through the collision energy as $\kappa = (2E/E_6^{00})^{1/2}$. Nonresonant capture in the (00) manifold then occurs in the field of a single effective AC (EAC) potential $EAC_{v^{00},J}(\rho)$ given by

$$EAC_{v^{00},J}(\rho) = \frac{J(J+1)}{2\rho^2} - \frac{1}{2\rho^6} \quad (3.1)$$

and the capture wave equation reads as

$$-\frac{1}{2} \frac{d^2 \psi^{00,J}}{d\rho^2} + EAC_{v^{00},J}(\rho) \psi^{00,J} = \frac{\kappa^2}{2} \psi^{00,J} \quad (3.2)$$

Since in this section we discuss only the (00) manifold, for simplicity of notation, we suppress superscripts 00. The solution of the above equation, with an absorbing boundary condition at small ρ , yields the capture probabilities $P^l(\kappa)$ and, from this, the scaled capture rate coefficients

$$\chi(\kappa) = \sum_{J=0}^{\infty} \chi^J(\kappa), \quad \chi^J(\kappa) = \frac{(2J+1)P^J(\kappa)}{2\kappa} \quad (3.3)$$

When J is replaced by l , this expression coincides with eq 14 of ref 10 for the rate coefficient of capture of structureless particles in the field of an attractive R^{-6} potential (for unscaled rate coefficients; see section 7 of this paper).

For $\kappa \ll 1$, the threshold expressions of the P^l are given by the analytical formulas:

$$P^l(\kappa) = \begin{cases} c_0 \kappa - (c_0 \kappa)^2/2 + O(\kappa^3) & \text{for } l = 0 \\ c_l \kappa^{2l+1} + O(\kappa^{2l+2}) & \text{for } l > 0 \end{cases} \quad (3.4)$$

where

$$c_l = \frac{8\pi^2}{(16)^s s^2 [\Gamma(s) \Gamma(s/2)]^2} \quad (3.5)$$

with $s = l + 1/2$.¹⁴ Note that $P^l(\kappa)|_{J=0}$ explicitly contains two terms rather than one, such as this is the case for $l > 0$ (see ref 11, section 143). Expression 3.4 conforms with the Bethe limit, yielding

$$\lim_{\kappa \rightarrow 0} \chi(\kappa) = c_0/2 = 0.956 \quad (3.6)$$

while the classical rate coefficient $^{\text{cl}}\chi(\kappa)$ vanishes with κ as $\kappa^{1/3}$.

For arbitrary κ , the approximate analytical expressions for $P^l(\kappa)$ are available up to $l = 4$.¹² Under conditions where the channel with $l = 3$ is classically open for capture, the relative accuracy of the classical approximation

$$^{\text{cl}}\chi(\kappa) = (3/4)(2\kappa)^{1/3} \quad (3.7)$$

is better than 5%. Graphs of $\chi(\kappa)$, $\chi^l(\kappa)$, and $^{\text{cl}}\chi(\kappa)$ vs κ are shown in sections 4 and 5 (Figures 3 and 8) though in a different scaling (the scaling length for the 00 manifold discussed here is R_6^{00} while that for the 01 manifold in sections 4 and 5 is R_6^{01}).

4. CAPTURE IN THE RESONANT MANIFOLD (01)

Capture in the 01 manifold is described by coupled equations which can be formulated either in jmJ or jlJ representation. Within the PR approximation for the interaction matrix, the coupling in the former representation is due to Coriolis interaction, while in the latter representation it is due to the off-diagonal part of the dipole–dipole interaction. The coupled equations in either representation have a simple structure as a consequence of the three integrals of motion, of total angular momentum (quantum number J), total parity (quantum number I), and permutation symmetry (quantum number p). For simplicity of notation, in this and the following sections we again suppress the superscripts 01 that specify the resonance manifold. The wave functions in the $jmJp$ representation do not necessarily correspond to definite total parity I , but they can be transformed by linear combinations of $|jmJp\rangle$ and $|j-mJp\rangle$ to new functions

$|jnI\rangle$ with $n = |m|$ and a certain I . The definite assignment for I' and I'' can be obtained after passage to the asymptotic region where l becomes a good quantum number. A general relation between the $|jnI\rangle$ and $|jl\rangle$ functions is provided by the vector addition rules¹³ slightly modified in their application to the parity-adapted basis (for a detailed discussion, see ref 14). For our case $j = 1$, these relations read as

$$|1, n, J, I', p\rangle|_{n=0} = \sqrt{\frac{J}{2J+1}} \times |1, l, J, p\rangle|_{l=J-1} - \sqrt{\frac{J+1}{2J+1}} \times |1, l, J, p\rangle|_{l=J+1} \quad (4.1a)$$

$$|1, n, J, I', p\rangle|_{n=1} = \sqrt{\frac{J+1}{2J+1}} \times |1, l, J, p\rangle|_{l=J-1} + \sqrt{\frac{J}{2J+1}} \times |1, l, J, p\rangle|_{l=J+1} \quad (4.1b)$$

$$|1, n, J, I'', p\rangle|_{n=1} = |1, l, J\rangle|_{l=J} \quad (4.1c)$$

which allows one to explicitly identify the total parity $I = (-1)^{l+j}$ through $I' = (-1)^J$, $I'' = -(-1)^J$. In what follows we adhere to the following convention: the quantum numbers which are the same for a given triplet of states (i.e., J, p) will appear as superscripts, while those which vary (i.e., m , or n, I , or l) as subscripts.

We now consider the coupled equations in the $jnI\rangle$ representation. Using the reduced variables $\rho = R/R_0^{01}$ and $\kappa = (2E/E_0^{01})^{1/2}$ with an additional parameter $\delta = \mu d^2/3\hbar^2 R_0^{01}$, we first write the effective AC (EAC) potentials in the $jmI\rangle$ basis as

$${}^{\text{Cl}}v_m^p(\rho; J, \delta) = \frac{J(J+1) + 2 - 2m^2}{2\rho^2} - \frac{1}{2\rho^6} + (3m^2 - 2)\frac{p\delta}{\rho^3} \quad (4.2)$$

with $m = 0, -1, +1$. In the $|jnI\rangle$ basis, the three potentials from eq 4.2 transform into ${}^{\text{EAC}}v_{n,I}^{J,p}$ with $n = 0, 1$ and $I = I', I''$:

$$\begin{aligned} {}^{\text{EAC}}v_{0,I'}^{J,p}(\rho; \delta) &= \frac{J(J+1) + 2}{2\rho^2} - \frac{1}{2\rho^6} - \frac{2p\delta}{\rho^3} \\ {}^{\text{EAC}}v_{1,I'}^{J,p}(\rho; \delta) &= \frac{J(J+1)}{2\rho^2} - \frac{1}{2\rho^6} + \frac{p\delta}{\rho^3} \\ {}^{\text{EAC}}v_{1,I''}^{J,p}(\rho; \delta) &= \frac{J(J+1)}{2\rho^2} - \frac{1}{2\rho^6} + \frac{p\delta}{\rho^3} \end{aligned} \quad (4.3)$$

The diagonal elements in eq 4.3 are supplemented by the off-diagonal Coriolis coupling between the states $|j0I\rangle$ and $|j1I\rangle$, i.e., by

$${}^{\text{C}}v_{I',I''}^J(\rho; \delta) = \frac{\sqrt{J(J+1)}}{\rho^2} \quad (4.4)$$

Equations 4.3 and 4.4 define the interaction matrix $\hat{Y}^{J,p}$ which, in the representation of the column vector radial wave function $\Psi^{J,p} = \{\psi_{0,I'}^{J,p}, \psi_{1,I'}^{J,p}, \psi_{1,I''}^{J,p}\}$, is of the form

$$\hat{Y}^{J,p} = \begin{pmatrix} {}^{\text{EAC}}v_{0,I'}^{J,p} & {}^{\text{C}}v_{I',I''}^J & 0 \\ {}^{\text{C}}v_{I',I''}^J & {}^{\text{EAC}}v_{1,I'}^{J,p} & 0 \\ 0 & 0 & {}^{\text{EAC}}v_{1,I''}^{J,p} \end{pmatrix} \quad (4.5)$$

The radial wave equation for $\Psi^{J,p}$ reads

$$-\frac{d^2}{2d\rho^2} \Psi^{J,p} + \hat{Y}^{J,p} \cdot \Psi^{J,p} = \frac{\kappa^2}{2} \Psi^{J,p} \quad (4.6)$$

By solving eq 4.6 with the capture boundary conditions (only an incoming wave for small ρ where the dipole–dipole interaction is stronger than the Coriolis coupling) and with standard boundary conditions for large ρ (only an incoming wave in one of the channels and outgoing waves in the other channels), for given J and p , three capture probabilities are determined, $\hat{P}^{J,p} = \{P_{0,I'}^{J,p}, P_{1,I'}^{J,p}, P_{1,I''}^{J,p}\}$. The general expression for the p -specific scaled energy-dependent rate coefficient $\chi^p(\kappa, \delta)$ in reduced variables and in this representation is

$$\chi^p(\kappa, \delta) = \frac{1}{6\kappa} \sum_{I=I',I''} \left\{ \sum_{n=0,1} \left[\sum_{J \geq n} (2J+1) P_{n,I}^{J,p}(\kappa, \delta) \right] \right\} \quad (4.7)$$

If the capture problem is formulated in the $jl\rangle$ representation and the respective capture probabilities $P_l^{J,p}$ are calculated, the expression for χ^p reads

$$\chi^p(\kappa, \delta) = \frac{1}{6\kappa} \sum_{J=0}^{\infty} \left[\sum_{l=|J-1|}^{J+1} (2J+1) P_l^{J,p}(\kappa, \delta) \right] \quad (4.8)$$

Note that, at the left-hand side of eq 4.8, the total parity quantum number I does not appear since it is determined by j and l as $I = (-1)^{j+l}$.

The p -averaged rate coefficient is given by

$$\chi(\kappa, \delta) = \frac{1}{2}(\chi^+(\kappa, \delta) + \chi^-(\kappa, \delta)) \quad (4.9)$$

Expression 4.9 for $\chi(\kappa, \delta)$ is valid for two incoherent initial states differing in p . If the initial state corresponds to a coherent superposition of two p -states (as, e.g., is the case for collision of a rotationally excited diatom with the corresponding ground-state diatom), eq 4.9 is valid under the additional assumption that the accumulated phase difference between different p -states does not affect the absorption at the complex boundary.

The probabilities $P_{n,I}^{J,p}$ in the $jnI\rangle$ representation are related to $P_l^{J,p}$ in the $jl\rangle$ representation by the unitary relation

$$\begin{aligned} P_l^{J,p}|_{l=J} &= P_{n,I'}^{J,p}|_{n=1} \\ P_l^{J,p}|_{l=J-1} + P_l^{J,p}|_{l=J+1} &= P_{n,I'}^{J,p}|_{n=0} + P_{n,I''}^{J,p}|_{n=1} \end{aligned} \quad (4.10)$$

This relation allows one to represent χ^p in a unified way as

$$\begin{aligned} \chi^p(\kappa, \delta) &= \sum_{J=0}^{\infty} \sum_{I=I',I''} \chi^{J,I,p}(\kappa, \delta) \\ \chi^{J,I,p}(\kappa, \delta) &= \frac{1}{6\kappa} (2J+1) P_l^{J,p}(\kappa, \delta) \end{aligned} \quad (4.11)$$

Here

$$\begin{aligned} P_l^{J,p}(\kappa, \delta) &= (P_l^{J,p}(\kappa, \delta)|_{l=J-1} + P_l^{J,p}(\kappa, \delta)|_{l=J+1}) \times \delta_{II'} \\ &\quad + P_l^{J,p}(\kappa, \delta)|_{l=J} \times \delta_{II''} \\ &= (P_{n,I'}^{J,p}(\kappa, \delta)|_{n=0} + P_{n,I'}^{J,p}(\kappa, \delta)|_{n=1}) \times \delta_{II'} \\ &\quad + P_{n,I''}^{J,p}(\kappa, \delta)|_{n=1} \times \delta_{II''} \end{aligned} \quad (4.12)$$

which is useful in displaying the partial structure of χ (see below). The partial contributions to χ can, therefore, be specified by triads of exact quantum numbers Jlp , i.e., the total angular momentum J , total parity I , and the permutation index p . For small κ , the capture probability in the $l=0$ channel will be a linear function of κ (the Bethe limit), while the probabilities with $l > 0$ will display a stronger κ dependence. We thus have

$$P_l^{J,p}(\kappa, \delta)|_{J=1, l=0, \kappa \rightarrow 0} = \alpha^p(\delta)\kappa \quad (4.13)$$

The given expressions simplify in the two limiting cases $\delta = 0$ and $\delta \gg 1$. For $\delta = 0$, eq 4.6 can be decoupled by a ρ -independent transformation of the AC basis. As a result, the probabilities $P_l^{J,p}$ with $|l-1| \leq J \leq l+1$ and $p = \pm$ become equal to each other, and the sum in eq 4.10, after regrouping, collapses into $\bar{\chi}^{J,p}(\kappa, \delta)|_{\delta=0} = (2l+1)P_l(\kappa)$, where $P_l(\kappa)$ is the capture probability for the potential $-1/2\rho^6$ and

$$\bar{\chi}^p(\kappa, \delta)|_{\delta=0} = \frac{1}{2\kappa} \sum_{l=0}^{\infty} (2l+1)P_l(\kappa) \\ P_l(\kappa) = P_l^{J,p}|_{J=l-1} = P_l^{J,p}|_{J=l} = P_l^{J,p}|_{J=l+1} \quad (4.14)$$

The counterpart of eq 4.13 reads

$$P_l(\kappa)|_{l=0, \kappa \rightarrow 0} = \alpha_0(\delta)\kappa \quad (4.15)$$

For $\delta \gg 1$, one may pass to new reduced variables $\tilde{\rho} = \rho/\delta$ and $\tilde{\kappa} = \kappa\delta$ and define the new scaled rate coefficient $\tilde{\chi}(\tilde{\kappa})$

$$\tilde{\chi}(\tilde{\kappa}) = \lim_{\delta \rightarrow \infty} \frac{\chi(\kappa, \delta)}{\delta} \quad (4.16)$$

The quantity $\tilde{\chi}(\tilde{\kappa})$ then is expressed via capture probabilities by equations similar to eqs 4.10–4.12; i.e.,

$$\tilde{\chi}^p(\tilde{\kappa}) = \sum_{J=0}^{\infty} \sum_{I=I', I''} \tilde{\chi}_I^{J,p}(\tilde{\kappa}) \\ \tilde{\chi}_I^{J,p}(\tilde{\kappa}) = \frac{1}{6\kappa} (2J+1) \tilde{P}_I^{J,p}(\tilde{\kappa}) \quad (4.17)$$

where

$$\tilde{P}_I^{J,p}(\tilde{\kappa}) = (\tilde{P}_I^{J,p}(\tilde{\kappa})|_{l=J-1} + \tilde{P}_I^{J,p}(\tilde{\kappa})|_{l=J+1}) \times \delta_{II'} \\ + \tilde{P}_I^{J,p}(\tilde{\kappa})|_{l=J} \times \delta_{II''} \\ = (\tilde{P}_{n,I'}^{J,p}(\tilde{\kappa})|_{n=0} + \tilde{P}_{n,I'}^{J,p}(\tilde{\kappa})|_{n=1}) \times \delta_{II'} \\ + \tilde{P}_{n,I''}^{J,p}(\tilde{\kappa})|_{n=1} \times \delta_{II''} \quad (4.18)$$

$$\tilde{P}_I^{J,p}(\tilde{\kappa})|_{J=1, l=0, \tilde{\kappa} \rightarrow 0} = \alpha_{\infty} \tilde{\kappa} \quad (4.19)$$

Here the $\tilde{P}_{n,I}^{J,p}(\tilde{\kappa})$ are calculated from the solution of the capture wave equation of eq 4.6 with the potentials from eqs 4.3 and 4.4, where ρ is replaced by $\tilde{\rho}$, κ by $\tilde{\kappa}$, δ is put equal to unity, and the term proportional to ρ^{-6} is disregarded. Note that $\tilde{\kappa}$ does not contain any information about a vanishing dispersion interaction and is expressed through the dipole moment d , the reduced mass μ and the wave vector k as $\tilde{\kappa} = \delta k = (d^2\mu/3\hbar^3)k$. It is thus clear that $\alpha_{\infty} = (\alpha(\delta)/\delta)|_{\delta \gg 1}$.

For the 00 manifold, the capture channels are decoupled, and the only quantum effect in the capture is the tunneling and overbarrier reflection of the collision partners across the

centrifugal barriers. The same feature happens for capture in the 01 manifold for $\delta = 0$ such that the rate coefficients for the former case are identical to those for the latter case provided that one takes into account a different scaling (length parameter R_0^{00} for the 00 manifold and R_0^{01} for the 01 manifold). Therefore we skip the discussion of the capture in the 00 manifold.

For the 01 manifold and $\delta \neq 0$, the capture channels are coupled, and the tunneling and overbarrier reflection occur on the background of nonadiabatic coupling which accompanies the locking of the intrinsic angular momentum to the collision axis. Each capture channel is specified by a triad of exact quantum numbers J, I, p and an additional quantum number \bar{l} that has the asymptotic meaning of the quantum number of the orbital angular momentum l . For the triad $J=0, I=+, p=\pm$, \bar{l} assumes the single value $\bar{l}=1$; for all other triads with $J \geq 1$, one has $\bar{l}=J-1, J, J+1$. With this definition of \bar{l} , the total parity quantum number becomes redundant since $I = -(-1)^{\bar{l}}$, and the set J, I, p, \bar{l} can be shortened to J, p, \bar{l} . In the following discussion of the rate coefficient for the 01 manifold, in section 5 we consider two limiting cases: capture at very small energy (the Bethe limit) and capture at energies high enough to fall into the category of the quantum-classical regime as defined by Billing,⁸ and in section 6 we consider the range between these limits.

5. LOW- AND HIGH-ENERGY LIMITS OF CAPTURE RATE COEFFICIENTS

For small κ , the largest capture probability is linear in κ , the respective cross-section is inversely proportional to κ , and the rate coefficient at $\kappa \rightarrow 0$ approaches a constant (Bethe limit), ${}^B\chi(\delta)$. We therefore have

$$\chi(\kappa, \delta)|_{\kappa \rightarrow 0} \equiv {}^B\chi(\delta) = \alpha(\delta)/2, \\ \alpha(\delta) = (\alpha^+(\delta) + \alpha^-(\delta))/2 \quad (5.1)$$

The plot of $\alpha(\delta)$, determined by numerical solution of the coupled equations discussed above, is shown in Figure 1 (solid line). Also shown is the analytical approximation, ${}^{\text{FW}}\alpha(\delta)$ (dashed line), that is derived from the fly wheel (FW) approach

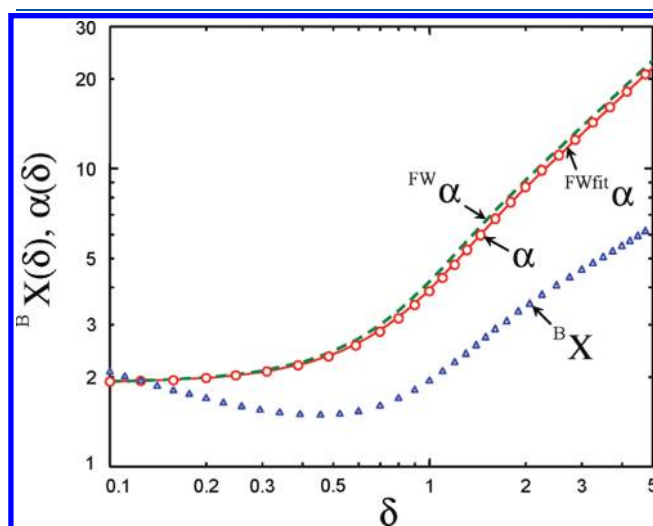


Figure 1. Graphs of ${}^{\text{FW}}\alpha(\delta)$ (dashed line), ${}^{\text{FWfit}}\alpha(\delta)$ (solid line) and $\alpha(\delta)$ (circles) as well as of the modified zero-energy quantum rate coefficient ${}^B\chi(\delta)$ (triangles). The latter plot represents an intersection of the function $K(\varepsilon, \delta)$ by the plane $\varepsilon = 0$ (see section 7 and Figure 13).

for an uncoupled channel with the FW potential:¹

$${}^{\text{FW}}v_{p,l=0}^{01} \equiv {}^{\text{FW}}v_0^{01}(\rho) = -\frac{1}{2\rho^6} \frac{2\delta^2}{3\rho^4} \quad (5.2)$$

The explicit expression for ${}^{\text{FW}}\alpha(\delta)$ reads as^{1,15}

$${}^{\text{FW}}\alpha(\delta) = 8|F(\delta)| \sin(\pi/4 - \arg F(\delta))$$

$$F(\delta) = \frac{\Gamma(3/4 - i\delta^2/3)}{\Gamma(1/4 - i\delta^2/3)} \quad (5.3)$$

We see from Figure 1 that the logarithmic graph of $\alpha(\delta)$ with high accuracy by a simple shift can be superimposed onto the graph of ${}^{\text{FW}}\alpha(\delta)$. To qualitatively understand this feature, we adhere to the picture of an uncoupled potential, just modifying its FW version by a diagonal nonadiabatic correction (DNC) which is known to be positive and equal to the expectation value of the operator $-\partial^2/2\partial\rho^2$ for an adiabatic wave function.¹⁶ In our case, this function, FWDNC, is this FW function ${}^{\text{FW}}|j=1, j=1, l=0\rangle$ augmented with a correction proportional to ${}^{\text{FW}}|j=1, j=1, l=2\rangle$. The coefficient $\gamma(\rho)$ in front of the latter is the ratio of the dipole–dipole interaction, $\propto \delta/\rho^3$, to the rotational energy difference between states with $l=0$ and $l=2$, $\propto l(l+1)/\rho^2$; i.e., $\gamma(\rho) \propto \delta/\rho$. Calculations similar to that outlined in section 7 of ref 16 yield

$$\langle \text{FWDNC} | -\partial^2/2\partial\rho^2 | \text{FWDNC} \rangle \propto (\partial\gamma/\partial\rho)^2 \propto \delta^2/\rho^4 \quad (5.4)$$

The correction from eq 5.4 together with the FW potential from eq 5.3 leads to the following expression for FWDNC potential

$${}^{\text{FWDNC}}v_{p,l=0}^{01} \equiv {}^{\text{FW}}v_0^{01}(\rho) = -\frac{1}{2\rho^6} \frac{2c^2\delta^2}{3\rho^4} \quad (5.5)$$

where the numerical coefficient c^2 is smaller than unity. This explains why the graph of ${}^{\text{FWDNC}}\alpha(\delta)$ (as well as $\alpha(\delta)$) which is presumably approximated by ${}^{\text{FWDNC}}\alpha(\delta)$ is simply shifted relative to ${}^{\text{FW}}\alpha(\delta)$ when plotted on logarithmic scale. The coefficient c^2 , of course, can be calculated within the above approach, but the respective quantity ${}^{\text{FWDNC}}\alpha(\delta) = {}^{\text{FW}}\alpha(c\delta)$ is not expected to provide a good approximation to $\alpha(\delta)$ since interchannel coupling is neglected. One could, however, consider c as a fitting parameter, ${}^{\text{fit}}c$, that would ensure the correct linear behavior of ${}^{\text{FW}}\alpha(\delta)|_{\delta \gg 1} \equiv {}^{\text{FW}}\alpha({}^{\text{fit}}c\delta)|_{\delta \gg 1} = (8/\sqrt{3}){}^{\text{fit}}c\delta = 4.619{}^{\text{fit}}c\delta$. A comparison with numerically determined $\alpha(\delta)|_{\delta \gg 1} = 4.367\delta$ yields ${}^{\text{fit}}c = 0.945$. Figure 1 presents graphs of ${}^{\text{FW}}\alpha(\delta)$, ${}^{\text{FWDNC}}\alpha(\delta)$, and $\alpha(\delta)$ which demonstrate the very good performance of the analytical approximation to $\alpha(\delta)$, $\alpha(\delta) \approx {}^{\text{FW}}\alpha(\delta) \equiv {}^{\text{FW}}\alpha({}^{\text{fit}}c\delta)$, and it shows that the FW approach represents a reasonable reference basis for a discussion of the effect of coupling on capture in the limit of low energies.

For future use, we introduce a modified Bethe rate coefficient as

$${}^{\text{B}}X(\delta) = \delta^{1/3} \times {}^{\text{B}}\chi(\delta) \quad (5.6)$$

The plot of ${}^{\text{B}}X(\delta)$ vs δ is also shown in Figure 1. For $\delta \ll 1$ and $\delta \gg 1$, the expressions for ${}^{\text{B}}X(\delta)$ are

$${}^{\text{B}}X(\delta) = \begin{cases} \alpha_0\delta^{-1/3}, & \delta \ll 1 \\ \tilde{\alpha}_\infty\delta^{2/3}, & \delta \gg 1 \end{cases} \quad (5.7)$$

Here α_0 is known from the analytical calculation for an uncoupled single channel, and α_∞ , from the present numerical calculations for coupled channels.

For large κ , when the rate coefficients are dominated by many partial channels, the relative motion in the majority of these channels is quasiclassical in the WKB sense, and the quantum rate coefficient χ should converge to its quantum-classical counterpart. Within this approach, the rotation of the dipoles is described quantum-mechanically while the relative motion is treated classically. A consistent quantum-classical theory would require some kind of blending of classical and quantum mechanics. This is a difficult task in the strong-coupling case, and a variety of approaches are available.⁸ The easiest one would be a common-trajectory approach, which, however, is not applicable to cases where the spacings between the states of the quantal subsystem (i.e., the spacing between AC potentials) are comparable or larger compared to the energy of the classical subsystem. In this situation we resort to the AC uncoupling between the perturbed rotor states and the states of relative motion, which allows us to treat the former quantum-mechanically and the latter classically. In suggesting this approach, we refer to our classical study of capture of j -specific dipolar molecules in an anisotropic R^{-3} potential, where the classical AC approach was shown to provide quite a good approximation to the numerically accurate results for rate coefficients of unpolarized rotors.^{4,5} Within this quantum-classical AC approach, which below simply will be called classical (superscript Cl), the capture rate coefficient is written as

$${}^{\text{Cl}}\chi = \frac{1}{12\kappa} \sum_{p=\pm} \sum_{m=0,\mp 1} \int_0^\infty 2J \text{d}J {}^{\text{Cl}}P_m^{J,p}(\kappa, \delta) \quad (5.8)$$

Here the capture probability is given by the step function Θ

$${}^{\text{Cl}}P_m^{J,p}(\kappa, \delta) = \Theta(\kappa - \kappa_m^p(J, \delta)) \quad (5.9)$$

in which the threshold wave vector $\kappa_m^p(J, \delta)$ is determined from the maximum of the effective potential:

$$(\kappa_m^p(J, \delta))^2/2 = \max\{{}^{\text{Cl}}v_m^p(\rho; J, \delta)\} \quad (5.10)$$

with

$${}^{\text{Cl}}v_m^p(\rho; J, \delta) = \frac{J^2}{2\rho^2} - \frac{1}{2\rho^6} + (3m^2 - 2)\frac{p\delta}{\rho^3} \quad (5.11)$$

Changing from κ to the classical scaled energy ε by the relation

$$\kappa = \delta\sqrt{\varepsilon}, \quad \varepsilon = E/E_*^{01}, \quad E_*^{01} = d^4/36C_6^{01} \quad (5.12)$$

we introduce the modified classical rate coefficient ${}^{\text{Cl}}X(\varepsilon)$ as

$${}^{\text{Cl}}X(\varepsilon) = \delta^{-1/3} \times {}^{\text{Cl}}\chi(\varepsilon, \delta) \quad (5.13)$$

Here

$${}^{\text{Cl}}X(\varepsilon) = \frac{1}{6}(X_{+2}(\varepsilon) + 2X_{+1}(\varepsilon) + 2X_{-1}(\varepsilon) + X_{-2}(\varepsilon)) \quad (5.14)$$

with

$$X_\nu(\varepsilon) = \frac{3}{2\kappa} \Phi^{1/3}(\varepsilon, \nu) [\Phi(\varepsilon, \nu) + \Delta] \Theta[\sqrt{\varepsilon} + \nu]$$

$$\Phi(\varepsilon, \nu) = \sqrt{\frac{\nu^2}{16} + \frac{\varepsilon}{2} - \frac{\nu}{4}} \quad (5.15)$$

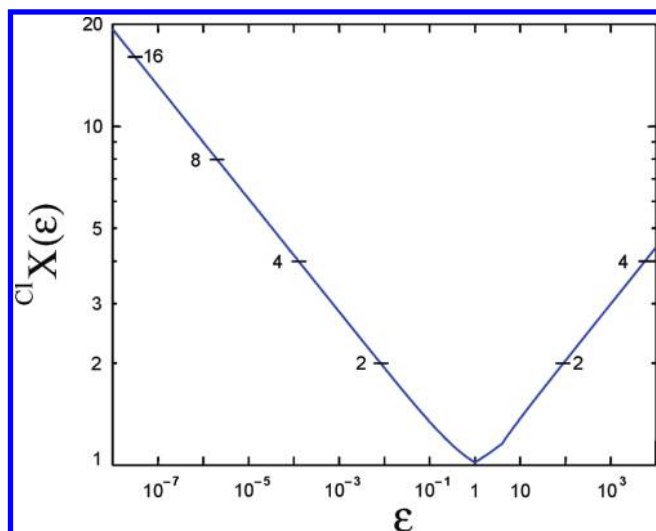


Figure 2. Graph of the modified classical rate coefficients ${}^{\text{Cl}}X(\varepsilon)$. This plot represents an intersection of the function $K(\varepsilon, \delta)$ by the plane $\delta = \text{constant} \gg 1$ (see section 7 and Figure 13).

where the step function $\Theta(x)$ closes the capture channels once the collision energy becomes less than the height of the barriers for those AC potentials which are asymptotically repulsive (negative ν). (Note that $\sqrt{3}$ in the argument of the Θ function in eq 16 of part I¹ is misprinted and should be removed.)

For $\varepsilon \ll 1$ and $\varepsilon \gg 1$, the expressions for ${}^{\text{Cl}}X(\varepsilon)$ are

$${}^{\text{Cl}}X(\varepsilon) = \begin{cases} (2 + 2^{2/3})\varepsilon^{-1/6}/4, & \varepsilon \ll 1 \\ 3(4\varepsilon)^{1/6}/4, & \varepsilon \gg 1 \end{cases} \quad (5.16)$$

The function ${}^{\text{Cl}}X(\varepsilon)$ attains its minimum at $\varepsilon = 1$, such that ${}^{\text{Cl}}X_{\text{min}} = 1.018$. A plot of this function is shown in Figure 2. The noticeable bend on the graph in the range $1 < \varepsilon < 10$ arises from the opening of channels with asymptotically repulsive interactions.

6. RATE COEFFICIENTS AT INTERMEDIATE ENERGIES. COMPARISON WITH ANALYTICAL APPROXIMATIONS

Advancing to the general case (arbitrary κ), in Figures 3–7 we show graphs of p -averaged rate coefficients $\chi(\kappa, \delta)$ vs κ (solid heavy line) and their partial terms $\chi_I^{J,p}(\kappa, \delta)$ (dotted and solid lines) for five representative choices of δ : $\delta = 0$, $\delta = 0.1$, $\delta = 1$, $\delta = 2$, and $\delta \gg 1$; the partial contributions are marked by the triads J, I, p . The appropriate comments to these figures are as follows.

Figure 3, $\delta = 0$, vanishing dipole–dipole interaction. Each capture channel is specified by l , and it is, in general, degenerate with respect to J and p . Explicitly, the degenerate components are as follows: triads $(1, -, \pm)$ for $l = 0$, triads $(0, +, \pm)$, $(1, +, \pm)$, $(2, +, \pm)$ for $l = 1$, triads $(1, -, \pm)$, $(2, -, \pm)$, $(3, -, \pm)$ for $l = 2$, and triads $(2, +, \pm)$, $(3, +, \pm)$, $(4, +, \pm)$ for $l = 3$, etc. The rate coefficient passes through a shallow minimum that separates two-channel and many-channel capture. The increase of $\chi(\kappa, \delta)|_{\delta=0}$ to the right from the minimum corresponds to a similar behavior of ${}^{\text{B}}X(\varepsilon)$ in Figure 2.

Figure 4, $\delta = 0.1$, weak dipole–dipole interaction. The degeneracy is slightly lifted, but for the two lowest capture channels the $p = +$ and $p = -$ splitting it is not discernible. The general pattern of $\chi(\kappa, \delta)|_{\delta=0.1}$ is similar to that of $\chi(\kappa, \delta)|_{\delta=0}$ in Figure 3.

Figure 5, $\delta = 1$, medium dipole–dipole interaction. The degeneracy is visibly lifted, and the minimum is more expressed.

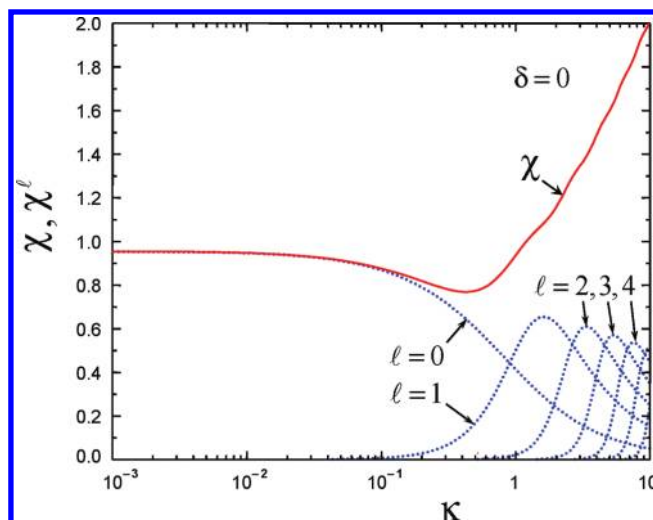


Figure 3. Graphs of rate coefficient $\chi(\kappa, \delta)$ vs κ (solid line) and the partial contributions $\chi_I^l(\kappa, \delta)$ (labeled by the values of l , dotted lines) for $\delta = 0$ and $l = 0, 1, 2, 3$, and 4.

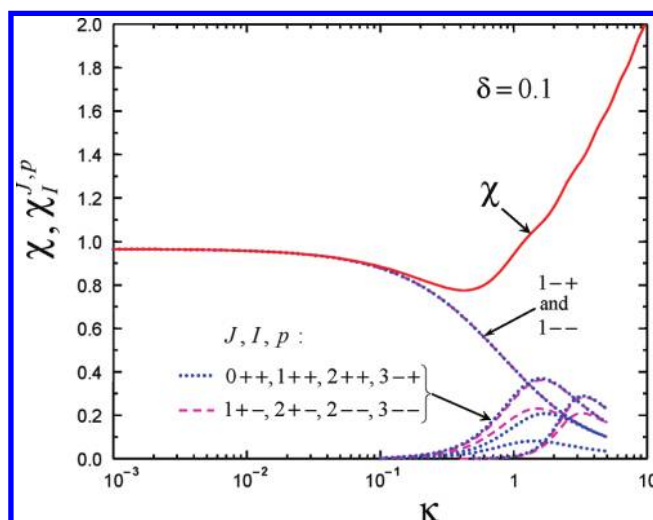
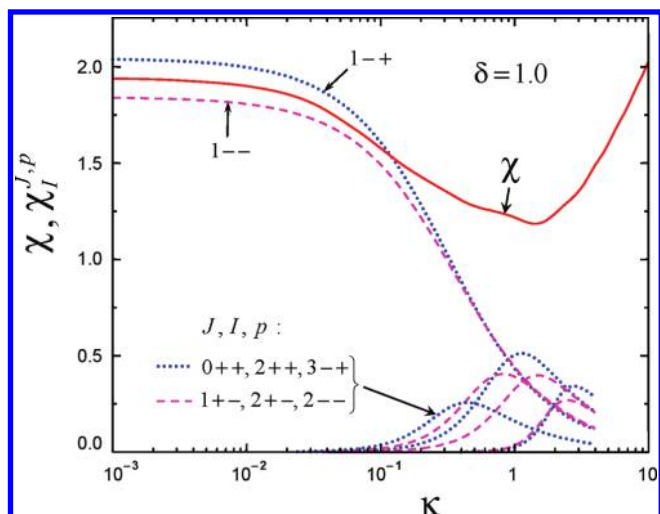
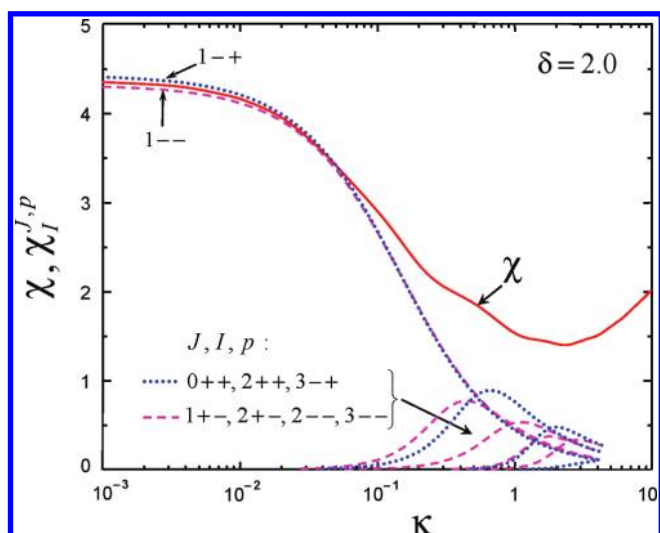
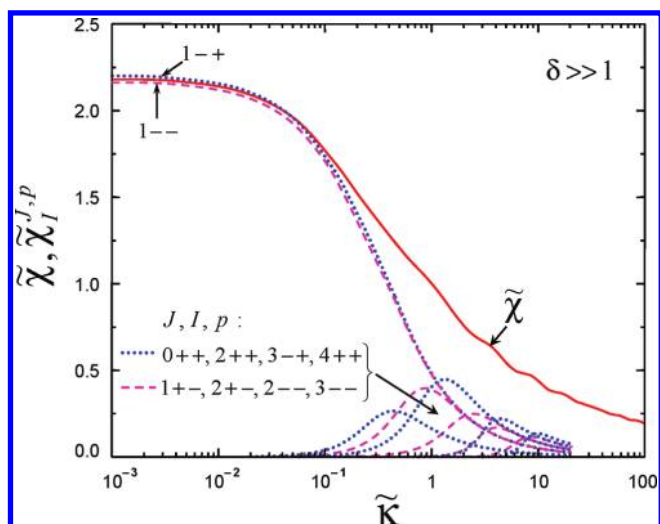
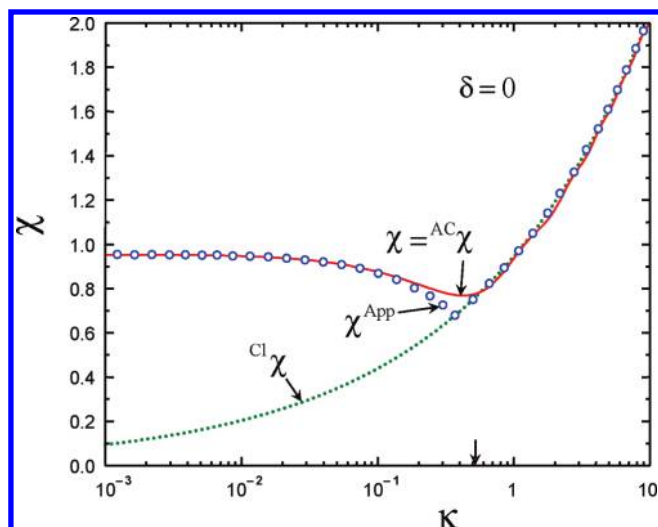
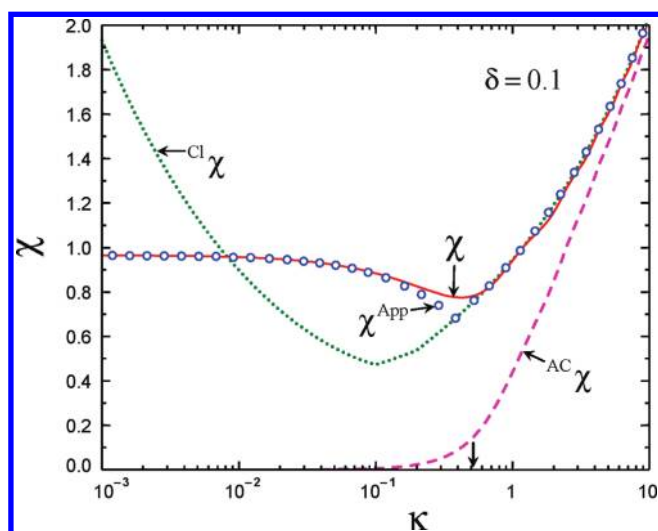


Figure 4. Graphs of the p -averaged rate coefficients $\chi(\kappa, \delta)$ vs κ (solid line) and their main partial contributions $\chi_I^{J,p}(\kappa, \delta)$ (labeled by triads J, I, p in the order of their appearance: dotted lines for $p = +1$ and dashed lines for $p = -1$) for $\delta = 0.1$ and $J = 0, 1, 2$, and 3. Partial contributions are not shown for $\kappa > 4$, where there are too many curves to be discernible in this figure. Note that the partial contributions with $I = I'$, which are expressed through two probabilities, each of sigmoid shape, do not show two maxima since the second one lies outside the displayed range of κ .

Otherwise, the general pattern of $\chi(\kappa, \delta)|_{\delta=1}$ is similar to that of $\chi(\kappa, \delta)|_{\delta=0.1}$ in Figure 3.

Figure 6, $\delta = 2$, medium dipole–dipole interaction. The general pattern of $\chi(\kappa, \delta)|_{\delta=2}$ is similar to that of $\chi(\kappa, \delta)|_{\delta=0.1}$ in Figure 5, except for a deeper minimum near the beginning of the increase of the rate.

Figure 7, $\delta \gg 2$, very strong dipole–dipole interaction. The minimum of $\chi(\kappa, \delta)|_{\delta \gg 1}$ within the range of κ shown disappears, and the rate in the many-channel capture regime corresponds to the negative energy dependence of ${}^{\text{B}}X(\varepsilon)$ in Figure 2 to the left from its minimum. Note that in this case half of the channels are closed for capture, such as this is also the case for ${}^{\text{B}}X(\varepsilon)$.

Figure 5. Same as Figure 4, but for $\delta = 1$.Figure 6. Same as Figure 4, but for $\delta = 2$.Figure 7. Same as Figure 4, but for $\delta \gg 1$.Figure 8. Convergence of the quantum rate coefficients $\chi(\kappa, \delta)$ (solid line) to their classical counterparts ${}^{\text{Cl}}\chi(\kappa, \delta)$ for $\delta = 0$ (dotted line, eq 3.7). Also shown are the analytical approximations $\chi^{\text{APP}}(\kappa, \delta)$ from eq 6.1 (symbols). The arrow marks the value of the wave vector at which the two branches of $\chi^{\text{APP}}(\kappa, \delta)$ from eq 6.1 approach each other.Figure 9. Same as Figure 8, but for $\delta = 0.1$.

The transition from the Bethe and to the classical limit, i.e., the convergence of $\chi(\kappa, \delta)$ (solid line) from its zero-energy limit ${}^{\text{B}}\chi(\delta)$ to ${}^{\text{Cl}}\chi(\kappa, \delta)$ (dotted line) is shown in Figures 8–12. For illustration of the importance of the Coriolis coupling, Figures 8–12 also show ${}^{\text{AC}}\chi$ (dashed curves), i.e., capture rate coefficients calculated within standard AC approximation by integration of eq 4.6 with off-diagonal terms disregarded. The vanishing of the AC rate coefficient in the limit $\kappa \rightarrow 0$ results from the κ^3 dependence of the largest capture probability in the tunneling through the lowest potential barrier of the effective AC potential $E_{\text{AC}}^{\text{EXC}} v_0^{0,+} = 1/\rho^2 - 2/\rho^3$. Two other features should be noted. First, the undulatory behavior of the quantum rate coefficients with respect to classical rate coefficients in Figures 6–9 is the counterpart of a similar behavior for capture in an isotropic potential such as that noted earlier.¹⁰ Second, with increasing collision energy the accurate rate coefficients $\chi(\kappa, \delta)$ converge to the classical AC rate coefficients ${}^{\text{Cl}}\chi(\kappa, \delta)$ for which the Coriolis

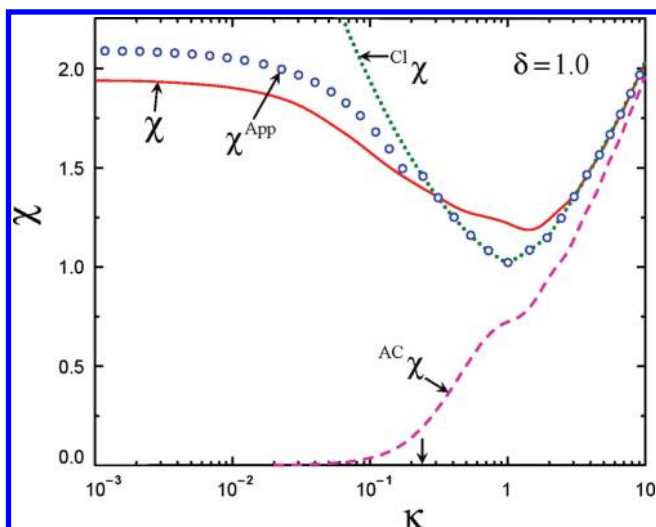


Figure 10. Same as Figure 8, but for $\delta = 1$.

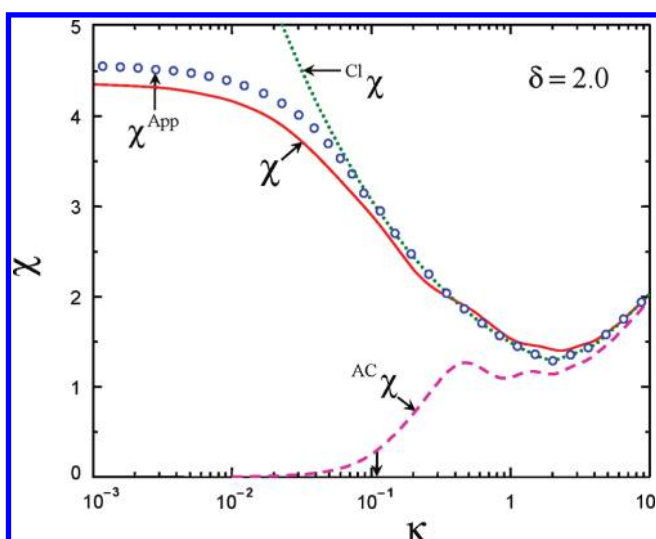


Figure 11. Same as Figure 8, but for $\delta = 2$.

coupling is neglected. This is consistent with the progressively weaker role of the rotational coupling in the region of passage across the centrifugal barriers with an increase of the total angular momentum. This observation applies, of course, to the capture of rotationally unpolarized molecules when the averaging over R -helicity projections, whether accomplished in the asymptotic region or in the region of the barriers, makes only a little difference.

Figures 8–12 also show a comparison of the accurate quantum rate coefficients and their analytical approximation suggested in part I¹ (symbols):

$$\chi^{\text{app}}(\kappa, \delta) = \begin{cases} \text{FW} \chi^{\text{TQK}}(\kappa, \delta), & \kappa < \kappa_c(\delta) \\ \text{Cl} \chi(\kappa, \delta), & \kappa > \kappa_c(\delta) \end{cases} \quad (6.1)$$

where $\text{Cl} \chi(\kappa, \delta)$ is given by eqs 5.8–5.11 and $\text{FW} \chi^{\text{TQK}}(\kappa, \delta)$ corresponds to the Troe–Quack–Klots (TQK) expression¹

$$\text{FW} \chi^{\text{TQK}}(\kappa, \delta) = \frac{1 - \exp(-\text{FW} \alpha(\delta) \kappa)}{2\kappa} \quad (6.2)$$

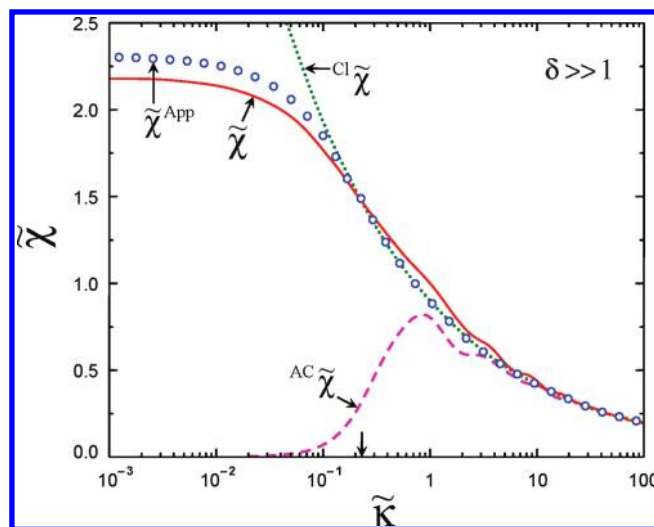


Figure 12. Convergence of the p -averaged quantum rate coefficients $\tilde{\chi}(\tilde{\kappa})$ (solid line) to their classical counterparts $\text{Cl} \tilde{\chi}(\tilde{\kappa})$ (dotted line, eq 6.5). Also shown is the analytical approximation $\tilde{\chi}^{\text{app}}(\tilde{\kappa}, \delta)$ from eq 6.4 (symbols) and the adiabatic channel approximation to the rate (dashed line). The arrow marks the value of the wave vector, at which the two branches of $\tilde{\chi}^{\text{app}}(\tilde{\kappa}, \delta)$ from eq 6.4 are closest to each other.

which conforms with the FW Bethe limit

$$\chi^{\text{B-FW}} = \frac{\text{B-FW} \alpha(\delta)}{2} \quad (6.3)$$

In eq 6.1, κ_c is the point of crossing or avoided crossing of the curves $\text{FW} \chi^{\text{TQK}}(\kappa, \delta)$ and $\text{Cl} \chi(\kappa, \delta)$. Approximately, $\kappa_c(\delta)$ can be estimated from the relation $\kappa_c(\delta) \approx 1/\text{FW} \alpha(\delta)$.

For $\delta \gg 1$, the counterpart of eq 6.1 is

$$\tilde{\chi}^{\text{app}}(\tilde{\kappa}) = \begin{cases} \text{FW} \tilde{\chi}_0^{\text{TQK}}(\tilde{\kappa}), & \tilde{\kappa} < \tilde{\kappa}_c \\ \text{Cl} \tilde{\chi}(\tilde{\kappa}), & \tilde{\kappa} > \tilde{\kappa}_c \end{cases} \quad (6.4)$$

with

$$\text{FW} \tilde{\chi}_0^{\text{TQK}}(\tilde{\kappa}) = \frac{1 - \exp\left(-\frac{8}{\sqrt{3}} \tilde{\kappa}\right)}{2\tilde{\kappa}} \quad (6.5)$$

$$\text{Cl} \tilde{\chi}(\tilde{\kappa}) = \frac{(2 + 2^{2/3})}{4} \tilde{\kappa}^{-1/3}$$

As an example, the small mismatch between $\text{FW} \tilde{\chi}_0^{\text{TQK}}(\tilde{\kappa})$ and $\text{Cl} \tilde{\chi}(\tilde{\kappa})$ at the point of the narrowly avoided crossing at $\tilde{\kappa}_c = 0.165$ equals 0.019; see Figure 10.

From Figures 10–12 we see that, at low energies, $\text{FW} \chi^{\text{TQK}}(\kappa, \delta)$ is larger than $\chi(\kappa, \delta)$. This can be ascribed to the effect of a coupling between the capture channels, in particular to the neglect of the diagonal positive correction¹⁶ to the attractive FW interaction that comes from the nonadiabatic radial coupling. The effect of the coupling gradually disappears with increasing collision energy since the transitions between coupled channels do not show up when many channels are equally populated in the asymptotic region.

7. DISCUSSION

In conventional units, the rate coefficients $k^{00}(E)$ and $k^{01}(E)$ as a function of the collision energy E read as

$$k^{\neq}(E) = \frac{2\pi\hbar R_6^{\neq}}{\mu} \chi^{\neq}(\kappa, \delta) \Big|_{\kappa = R_6^{\neq} \sqrt{2\mu E}/\hbar} \quad (7.1)$$

where \neq stands for 00 or 01, $R_6^\neq = (2\mu C_6^\neq/\hbar^2)^{1/4}$, and $\delta = 0$ for the 00 manifold.

Using eq 5.13 for ^{Cl}k , we write the classical rate coefficient as

$$^{Cl}k^\neq(\varepsilon) = 2\sqrt{2}\pi \times \mu^{-1/2} (C_6^\neq)^{1/3} (E_*^\neq)^{1/6} \times ^{Cl}X(\varepsilon) \quad (7.2)$$

where $\varepsilon = E/E_*^\neq$. The conditions $\varepsilon > 1$ and $\varepsilon < 1$ determine whether capture occurs mainly in the field of the isotropic ($\approx R^{-6}$) or anisotropic ($\approx R^{-3}$) interaction (for the 00 manifold, only the former is true since $E_*^\neq = 0$). With decreasing energy, $^{Cl}k^{01}(\varepsilon)$ first decreases and then, passing the point $\varepsilon = 1$, begins to increase. On this way, $^{Cl}k^{01}$ comes close to (or crosses) the rate coefficient $^{FW}k^{TQK}$ which reads as

$$^{FW}k^{TQK}(\varepsilon) = \frac{2\pi\hbar R_6^{01}}{\mu} \frac{[1 - \exp(-^{FW}\alpha(\delta)\delta\sqrt{\varepsilon})]}{2\delta\sqrt{\varepsilon}} \quad (7.3)$$

At this point, k^{01} switches from ^{Cl}k to $^{FW}k^{TQK}$, and the transition, according to eq 7.3, occurs at the energy $E \approx E_c^{01} = E_*^\neq / ^{FW}\alpha^2(\delta)\delta^2$. Whether the quantum regime with decreasing energy is reached on the decreasing or increasing branch of the classical rate $^{Cl}k^{01}$ depends on the value of the product $^{FW}\alpha(\delta)\delta$. For $^{FW}\alpha(\delta)\delta < 1$ it occurs on the decreasing branch, and for $^{FW}\alpha(\delta)\delta > 1$, on the increasing branch. With a further decrease of the energy, $k(E)$ tends to its Bethe limit, given approximately as

$$Bk^{01} = \frac{\pi\hbar R_6^{01}}{\mu} \alpha(\delta) \approx B^{-FW}k^{01} = \frac{\pi\hbar R_6^{01}}{\mu} ^{FW}\alpha(\delta) \quad (7.4)$$

To see the explicit dependence of $B^{-FW}k^{01}$ on interaction parameters, as suggested in part I,¹ we can use an approximate expression for $^{FW}\alpha(\delta)$ which reasonably well extrapolates between the exact limits at $\delta = 0$ and $\delta \gg 1$ from eq 5.3:

$$^{FW}\alpha(\delta) \approx 4\{(0.479)^6 + (2\delta/\sqrt{3})^6\}^{1/6} \quad (7.5)$$

Collecting the factors of eq 7.4, we get

$$B^{-FW}k^{01} \approx 4\pi \left\{ (0.479)^6 \left(\frac{2C_6^{01}\hbar^2}{\mu^3} \right)^{3/2} + \left(\frac{2d^2}{3\sqrt{3}\hbar} \right)^6 \right\}^{1/6} \quad (7.6)$$

For the description of different regimes of the capture one may use three characteristic energies: the rotational constant of the diatom (in energy units), B ; the energy $E = E_*^{01}$ that defines the minimum of the classical capture rate, $E_*^{01} = d^4/36C_6^{10}$; and the energy $E = E_c$ that defines the onset of the quantum regime in the capture, $E_c^{01} = E_*^\neq / ^{FW}\alpha^2(\delta)\delta^2 = E_6^{01}/2^{FW}\alpha^2(\delta)$. The conditions imposed on the value of the collision energy in the different regimes are as follows: (i) $E < B$, applicability of the PR approximation; (ii) $E > E_*^{01}$, capture mainly in the field of the isotropic R^{-6} attraction, positive energy dependence of the rate coefficient; (iii) $E < E_*^{01}$, capture mainly in the field of the anisotropic R^{-3} attraction, negative energy dependence of the rate coefficient; (iv) $E > E_c^{01}$, classical capture, positive or negative energy dependence of the rate coefficient; (v) $E < E_c^{01}$, quantum capture, weak negative energy dependence of the rate coefficient leading to the Bethe limit at $E = 0$.

The qualitative features of the rate coefficient can be illustrated by a plot of the scaled rate coefficient $K(\varepsilon, \delta)$ above the plane of the coordinates ε, δ . The quantity $K(\varepsilon, \delta)$ is defined as $^{Cl}X(\varepsilon)$ in the classical region, while in the quantum region it has the Bethe

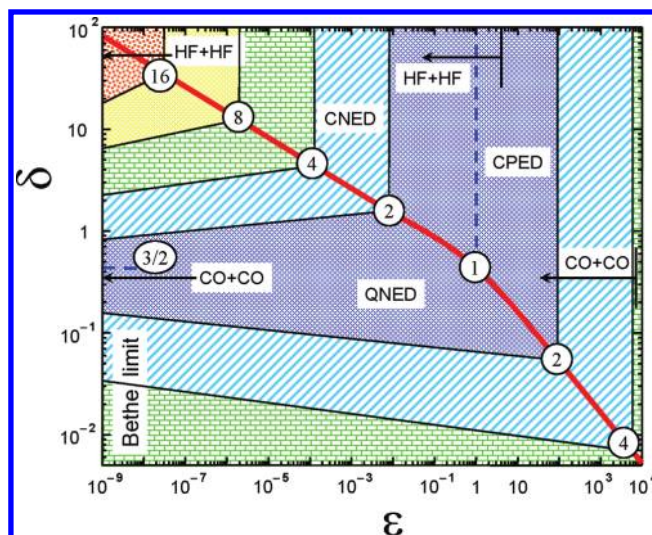


Figure 13. Equal- K lines of the scaled rate coefficients $K(\varepsilon, \delta)$ above the plane of the coordinates ε, δ . The heavy solid line separates the classical and quantum regions. Encircled numbers mark the values of $K(\varepsilon, \delta)$. Two cases discussed (CO + CO and HF + HF capture) correspond to the regions in the direction of the arrows. (See text for more details.)

limit $K(\varepsilon, \delta)_{\varepsilon \rightarrow 0} = B^X(\delta)$ that is obtained from the comparison of eq 5.6 and eq 5.13. Two sections of the surface $K(\varepsilon, \delta)$, $B^X(\delta)$ vs δ and $^{Cl}X(\varepsilon)$ vs ε , are shown in Figures 1 and 2, respectively. This allows one to qualitatively construct a set of level lines of $K(\varepsilon, \delta)$ that cover three regions with different energy dependence (ED) of the rate coefficients (classical positive ED, CPED, classical negative ED, CNED, and quantum negative ED, QNED); see Figure 13. The value of $K(\varepsilon, \delta)$ on a particular level line is marked at the boundary (the heavy line) between the classical and quantum regions defined by the equation $\varepsilon = \alpha^2(\delta)\delta^2$. The vertical δ -independent level lines in the CPED and CNED regions are those for the function $X(\varepsilon)$ (the minimum value of $X(\varepsilon)$ is put here as 1, instead of the accurate value 1.018). The straight slanted level lines in the QNED region, which simulate slightly curved accurate lines, were drawn by joining points at the ordinate axis (calculated from eq 6.3) with appropriate points at the quantum-classical boundary. The color of the strips of the table-of-contents figure, encompassed by two neighboring level lines, changes, in the rainbow sequence, from dark blue around the minimum (about 1 in the classical region and 3/2 in the quantum region) to red (left upper corner) for high values of $K(\varepsilon, \delta)$. Two examples for capture events are discussed in the following. These examples are marked by arrows which start to the left from two vertical lines that correspond to the ratios $\varepsilon_B = B/E_*^{01}$ for the molecules CO and HF.

We now consider in more detail two examples, capture in the encounters CO + CO and HF + HF. These two capture events represent extremes in the row of dipole molecules with respect to the values of the parameter δ that affects capture in the resonance manifold of channels. The relevant parameters for these, and also for “intermediate” systems such as HCl–HCl and HBr–HBr, are compiled in Tables 1–3 (see also the two arrows in Figure 13 for CO–CO and HF–HF collisions which bracket the respective arrows for HCl–HCl and HBr–HBr). For CO, the dipole moment is very small, and the dipole–dipole correction to the dispersion interaction is negligible. For 00 capture and

Table 1. Molecular Parameters Used in the Calculation

parameters ^a	CO	HF	HCl	HBr
mass of molecule	28 amu	20 amu	36 amu	81 amu
μ	14.0 amu = 2.55×10^4 au	10.0 amu = 1.82×10^4 au	18.0 amu = 3.28×10^4 au	40.5 amu = 7.38×10^4 au
d	0.1098 D = 1.098×10^{-19} esu cm = 0.0432 au	1.826 D = 1.826×10^{-18} esu cm = 0.718 au	1.109 D = 1.109×10^{-18} esu cm = 0.436 au	0.8272 D = 8.272×10^{-19} esu cm = 0.325 au
B	1.925 cm ⁻¹ = 2.77 K = 8.77×10^{-6} au	20.96 cm ⁻¹ = 30.16 K = 9.55×10^{-5} au	10.59 cm ⁻¹ = 15.24 K = 4.83×10^{-5} au	8.465 cm ⁻¹ = 12.18 K = 3.86×10^{-5} au
C_6 ^b	87.0 au = 83.3 $\times 10^{-60}$ erg cm ⁶	110 au = 105 $\times 10^{-60}$ erg cm ⁶	110 au = 105 $\times 10^{-60}$ erg cm ⁶	184 au = 176 $\times 10^{-60}$ erg cm ⁶

^a μ = reduced mass; d = dipole moment; B = rotation constant; C_6 = dispersion coefficient. ^b Comment: The values of the dispersion coefficient for CO, HCl, and HBr are taken from ref 17; this parameter for HF is assumed to be the same as that for HCl.

Table 2. Parameters That Enter into the Rate Coefficients for 00 Capture

parameters ^a	CO	HF	HCl	HBr
γ_{00}	7.60×10^{-4}	4.22	1.13	0.262
effective C_6^{00} , au	87.1	574	235	232
R_6^{00} , a_0	45.9	67.6	62.6	76.5
E_6^{00} , K	5.87×10^{-3}	3.78×10^{-3}	2.45×10^{-3}	7.30×10^{-4}
E_{00}^{quant} , K	8.03×10^{-4}	5.18×10^{-4}	3.35×10^{-4}	1.00×10^{-4}
B_k^{00} , cm ³ s ⁻¹	6.62×10^{-11}	1.37×10^{-10}	7.02×10^{-11}	3.81×10^{-11}

^a C_6 = dispersion coefficient; B_k^{00} = Bethe limit.

Table 3. Parameters That Enter into the Rate Coefficients for 01 Capture

parameters ^a	CO	HF	HCl	HBr
δ	0.346	53.8	36.2	35.0
γ_{01}	3.38×10^{-4}	1.87	0.504	0.116
effective C_6^{01} , au	87.0	316	165	205
R_6^{01} , a_0	45.9	58.3	57.4	74.2
E_6^{01} , K	5.87×10^{-3}	5.10×10^{-3}	2.92×10^{-3}	7.76×10^{-4}
E^{class} , K	3.51×10^{-4}	7.37	1.92	0.476
E_{01}^{quant} , K	6.30×10^{-4}	4.14×10^{-8}	5.22×10^{-8}	1.48×10^{-8}
Bethe limit $B_k^{01}(\delta)$, cm ³ s ⁻¹	7.47×10^{-11}	1.527×10^{-8}	5.63×10^{-9}	3.13×10^{-9}
$\eta = B_k^{01}(\delta)/B_k^{01}(0)$	1.13	169	97.0	87.0

^a C_6 = dispersion coefficient; B_k^{00} = Bethe limit.

energies E noticeably below $B_{\text{CO}} = 2.77$ K, e.g., decreasing from tenths of kelvin (case i), the classical rate coefficient decreases with energy (case ii) until $E = E_c^{00} = 8 \times 10^{-4}$ K. After that, it slowly increases (case v), approaching the Bethe limit B_k^{00} (CO–CO) = 6.62×10^{-11} cm³ s⁻¹. For 01 capture, with the parameter δ being rather small, $\delta = 0.346$, the classical rate coefficient also decreases with energy (case ii) down to $E^* = 3.5 \times 10^{-4}$ K. However, before reaching the turnover energy $E_c^{01} = 3.5 \times 10^{-4}$ K, at an energy equal to $E_c^{01} = 6.3 \times 10^{-4}$ K the quantum regime sets on. Therefore, the classical increase for $E < E_c^{01}$ does not occur at all, and it is replaced by the much weaker quantum increase for $E < E_c^{01}$ (case iv) that leads to the Bethe limit which is only slightly larger (by about 13%) than that for unpolar molecules.

For HF, the dipole moment is quite large, and the dipole–dipole correction to the dispersion interaction exceeds the latter. For 00 capture, for energies E noticeably below $B_{\text{HF}} = 30.16$ K, e.g., decreasing from 1 K (case i), the classical rate coefficient decreases with energy (case ii) until

$E = E_c^{00}(\text{HF–HF}) = 5.18 \times 10^{-4}$ K which is slightly below $E_c^{00}(\text{CO–CO})$ due to a larger value of R_6^{00} . For 01 capture, the parameter δ is quite large, $\delta = 53.8$. The energy E_c^{01} is about 4 orders of magnitude higher than the respective value for CO–CO and only four times smaller than $B_{\text{HF}} = 30.16$ K. Therefore, for energies E below, e.g., 1 K (case i), the rate coefficient increases with decreasing energy (case ii) until E reaches E_c^{01} which is substantially lower than its counterpart for CO–CO capture. The physical reason for the relation $E_c^{01}(\text{HF–HF}) \ll E_c^{01}(\text{CO–CO})$ in a situation where the reduced masses and dispersion coefficients are quite comparable is due to the fact that the WKB conditions for a gradual interaction (R^{-3} for HF–HF) break down at lower energies than for a steeper interaction (R^{-6} for CO–CO). When E becomes lower than E_c^{01} , the classical increase of the rate coefficient, as $E^{-1/6}$, changes into a much weaker quantum increase that leads to the Bethe limit at $E = 0$. The latter is larger than for unpolar molecules by the factor $(C_6^{01}/C_6)^{1/4} \times [\alpha(\delta)/\alpha(0)] = 169$.

8. CONCLUSIONS

One can draw the following conclusions from the given discussion.

(i) The capture of dipoles in the ground nonresonant state ($j_1 = 0, j_2 = 0$) occurs in a manifold of decoupled channels in the field of attractive dispersion and second-order dipole–dipole potentials. Here, quantum effects in the capture are due to adiabatic tunneling and overbarrier reflection during the passage of effective centrifugal barriers. The *s*-wave quantum capture leads to a finite limiting zero-energy rate coefficient, in contrast to a vanishing classical rate. Supplemented with classical rate coefficients for higher energies, the *s*-wave capture contribution satisfactorily describes the energy dependence of the rate across the whole energy range.

(ii) The capture of dipoles in the first excited resonant state ($j_1 = 0, j_2 = 1, 0$) occurs in a manifold of coupled channels in the field of the attractive/repulsive first-order dipole–dipole interaction potentials superimposed onto the attractive dispersion and second-order dipole–dipole potentials. Here, the quantum effects are due to a locking of the intrinsic angular momentum of the rotating molecules to the collision axis and to nonadiabatic tunneling and overbarrier reflection in the locking region. The “*s*-wave” (i.e., *s*-wave type) quantum capture leads to a finite limiting zero-energy rate coefficient, in contrast to the diverging classical rate. Supplemented with classical adiabatic channel rate coefficients for higher energies, the *s*-wave capture contribution satisfactorily describes the energy dependence of the rate across the whole energy range.

(iii) The analytical approximations of part I of this work¹ satisfactorily reproduce the close-coupling results. For $E < E_c$, the accurate quantum rate coefficients for rotationally unpolarized colliders are dominated by *s*-wave capture, which in the limit of $E \rightarrow 0$ with accuracy better than 10% is described by the analytical fly wheel approximation. The slight overestimation of the accurate rate by FW approach is due to a coupling effect, in particular to the neglect of the diagonal positive correction to the attractive FW interaction that comes from the nonadiabatic radial coupling.¹⁶ For $E > E_c$, the accurate quantum rate coefficient quite quickly converges to its quantum-classical counterpart.

(iv) For the capture of dipoles in the resonant state, the standard adiabatic channel (or coupled state) method is inadequate for a calculation of the rate coefficient at energies below about E_c .

(v) Two given examples, CO + CO and HF + HF capture, illustrate a wide range of conditions that can occur in the capture of two identical dipolar diatomic molecules, one of which is rotationally excited. The three regions in Figure 13, CPEN, CNED, and QNED, correspond to different energy dependences (ED) of the rate coefficients (classical positive ED, classical negative ED, and quantum negative ED), and the level lines qualitatively characterize the ED of the rate coefficient.

(vi) The results obtained apply as well to the transient formation of molecular species from two atoms, interacting via resonance dipole–dipole interaction, at very low collision energy. In a way, this represents a kind of a quantum reflection model such as discussed for van der Waals interactions in ref 18.

AUTHOR INFORMATION

Corresponding Author

*E-mail: shoff@gwdg.de.

ACKNOWLEDGMENT

Financial support of this work by the Deutsche Forschungsgemeinschaft (Project TR 69/17-1) is gratefully acknowledged.

GLOSSARY OF TERMS

Abbreviations:

AC	adiabatic channel
C	cociolis
CC	close coupling
CS	coupled states
Cl	classical
CPED	classical positive energy dependence
CNED	classical negative energy dependence
EAC	effective adiabatic channel
ED	energy dependence
FW	fly wheel
PR	perturbed rotor
QC	quantum-classical
QNED	quantum negative energy dependence
TQK	Troe–Quack–Klots

Probabilities (Partial Rate Coefficients):

$P^{J,L,P}(\chi^{J,L,P})$

cumulative capture probabilities (partial rate coefficients)

$P_{n,l}^{j,p}(\chi_{n,l}^{j,p})$ capture probability (partial rate coefficients) in the $jnJl$ representation

$P_1^{j,p}(\chi_1^{j,p})$ capture probability (partial rate coefficients) in the jl representation

REFERENCES

- (1) Nikitin, E. E.; Troe, J. *Phys. Chem. A* **2010**, *114*, 9762.
- (2) Auzinsh, M.; Dashevskaya, E. I.; Litvin, I.; Nikitin, E. E.; Troe, J. *J. Chem. Phys.* **2008**, *128*, 184304.
- (3) Auzinsh, M.; Dashevskaya, E. I.; Litvin, I.; Nikitin, E. E.; Troe, J. *J. Chem. Phys.* **2009**, *130*, 014304.
- (4) Dashevskaya, E. I.; Litvin, I.; Nikitin, E. E. *J. Phys. Chem. A* **2006**, *110*, 2786.
- (5) Dashevskaya, E. I.; Litvin, I.; Nikitin, E. E.; Troe, J. *Mol. Phys.* **2010**, *108*, 873.
- (6) Alexander, M. H.; Rackham, E. J.; Manolopoulos, D. E. *J. Chem. Phys.* **2004**, *121*, 5221.
- (7) Atahan, S.; Alexander, M.; Rackham, E. J. *J. Chem. Phys.* **2005**, *123*, 204306-1.
- (8) Billing, G. T. *The Quantum Classical Theory*; Oxford University Press: Oxford, U.K., 2003.
- (9) Hirschfelder, J. O.; Curtiss, C. F.; Bird, R. B. *Molecular Theory of Gases and Liquids*; John Wiley and Sons: New York, 1954.
- (10) Dashevskaya, E. I.; Litvin, I.; Maergoiz, A.; Nikitin, E. E.; Troe, J. *J. Chem. Phys.* **2003**, *118*, 7313.
- (11) Landau, L. D.; Lifshitz, E. M. *Quantum Mechanics*; Pergamon Press: Oxford, U.K., 1977.
- (12) Dashevskaya, E. I.; Litvin, I.; Nikitin, E. E.; Troe, J. *Phys. Chem. Chem. Phys.* **2009**, *11*, 9364.
- (13) Zare, R. N. *Angular Momentum*; John Wiley and Sons: New York, 1988.
- (14) Shternin, P. S.; Vasyutinskii, O. S. *J. Chem. Phys.* **2008**, *128*, 194314.
- (15) Eltschka, C.; Moritz, M.; Friedrich, H. *J. Phys. B: At., Mol. Opt. Phys.* **2000**, *33*, 4033.
- (16) Nikitin, E. E.; Umanskii, S. Ya. *Theory of Slow Atomic Collisions*; Springer: Berlin, 1984.
- (17) *CRC Handbook of Chemistry and Physics*; Lide, D. R., Hanes, W. M., Eds.; CRC Press: New York, 2009.
- (18) Dickinson, A. S. *J. Phys. B: At., Mol. Opt. Phys.* **2007**, *40*, F237.